







MERIDIONAL OCEANIC AND ATMOSPHERIC HEAT FLUXES AT THE ENTRANCE TO THE ATLANTIC SECTOR OF THE ARCTIC: VERIFICATION OF CMIP6 MODELS AND CLIMATE PROJECTIONS BASED ON THE SELECTED SUB-ENSEMBLES

M. M. Latonin^{1,2,*} , I. L. Bashmachnikov^{1,2} , Iu. V. Radchenko¹ ,
N. V. Gnatiuk^{1,2} , L. P. Bobylev¹ , and L. H. Pettersson³ 

¹Nansen International Environmental and Remote Sensing Centre, Saint Petersburg, Russia

²Saint Petersburg State University, Saint Petersburg, Russia

³Nansen Environmental and Remote Sensing Center, Bergen, Norway

* **Correspondence to:** Mikhail M. Latonin, mikhail.latonin@niersc.spb.ru

Abstract: Poleward transports of oceanic and atmospheric heat play an essential role in the Arctic climate system, and their variations in the future will strongly shape the climate of the Arctic. The main aim of this study is to evaluate the performance of the Coupled Model Intercomparison Project phase 6 (CMIP6) models in the historical experiment in simulating the meridional heat fluxes into the Atlantic sector of the Arctic. The secondary objective is to estimate the meridional oceanic and atmospheric heat fluxes up to the end of the 21st century using the best sub-ensembles of the CMIP6 models. According to our results, the CMIP6 models poorly reproduce the interannual variability of the heat fluxes in their historical simulations, and the multi-model ensemble mean values are systematically lower than the mean values derived from the Ocean ReAnalysis System 4 (ORAS4) and European Centre for Medium-Range Weather Forecasts Reanalysis version 5 (ERA5) reanalyses. Climate projections based on the selected CMIP6 models indicate that the future Arctic climate will be characterized by the significantly increased oceanic heat transport at the entrance to the Atlantic sector of the Arctic relative to the period 1958–2014. In contrast, the atmospheric heat and moisture transport will not have dramatic differences in the projected Arctic climate relative to the period 1958–2014. Based on the results obtained, we emphasize that any interpretation of future climate simulations should be done with caution.

Keywords: poleward heat transport, climate of the Arctic, ocean–atmosphere interaction, CMIP6 models, ORAS4 and ERA5 reanalyses, projections, North Atlantic.

Citation: Latonin, M. M., I. L. Bashmachnikov, Iu. V. Radchenko, N. V. Gnatiuk, L. P. Bobylev, and L. H. Pettersson (2024), Meridional Oceanic and Atmospheric Heat Fluxes at the Entrance to the Atlantic Sector of the Arctic: Verification of CMIP6 Models and Climate Projections Based on the Selected Sub-Ensembles, *Russian Journal of Earth Sciences*, 24, ES4007, EDN: CISMVQ, <https://doi.org/10.2205/2024es000917>

RESEARCH ARTICLE

Received: 26 October 2023

Accepted: 8 July 2024

Published: 31 October 2024



Copyright: © 2024. The Authors. This article is an open access article distributed under the terms and conditions of the Creative Commons Attribution (CC BY) license (<https://creativecommons.org/licenses/by/4.0/>).

1. Introduction

One of the essential components of the Arctic climate system is the energy (heat) exchange with lower latitudes [Serreze and Barry, 2014]. The on-going global warming, amplified in the Arctic, is projected to continue in the 21st century [Esau et al., 2023; Koenigk et al., 2012; Liang et al., 2020]. The annual surface and atmospheric energy budget to the north of the Arctic circle is largely driven by the heat transport in the ocean and atmosphere. The warmer upper ocean gradually releases its heat to the atmosphere, while the thickness of the mixed layer is increasing with winter convection [Lique et al., 2017]. The atmospheric heat transport is largely driven by extratropical cyclones [Alexeev et al., 2017]. The North Atlantic is a region where there is a strong poleward heat transport both in the atmosphere and the ocean [Graham et al., 2017; Madonna and Sandø, 2021]. This is also a “hotspot” of ocean–atmosphere interaction, which was originally noted in [Bjerknes,

1964] and proved to be the case in many subsequent studies, [e.g., [Outten et al., 2018](#); [van der Waluw et al., 2007](#)]. One of the implications of the horizontally advected oceanic heat into the Arctic is a subsequent change in the vertical heat flux. For instance, numerical ice-ocean models applied in [[Polyakov et al., 2010](#)] showed that an increased oceanic heat flux due to the presence of warm Atlantic water makes the sea ice substantially thinner in the Arctic Ocean. In addition, the atmosphere has a strong impact on the Arctic sea ice by wind forcing, which further triggers the local surface albedo feedback [[Zhang et al., 2008](#)]. It was also found that warm and moist air intrusions into the Atlantic sector of the Arctic have had a leading role in winter warming events in the Arctic since 1954 [[Graham et al., 2017](#)]. Overall, it is difficult to distinguish whether the oceanic or atmospheric warming is dominant in the Atlantic sector of the Arctic. This region is commonly defined up to the North Pole in the western part of the Arctic adjacent to the subpolar North Atlantic, and the eastern border is defined by the Kara Sea.

Although the impacts of poleward oceanic and atmospheric heat transport are widely debated both in the past and future perspectives [[Goosse et al., 2018](#)], there is no one standard for the calculation of heat transport in the ocean and atmosphere. The oceanic heat transport is often calculated with the reference temperature and using the temperature scale in degrees Celsius [[Docquier and Koenigk, 2021](#); [Årthun et al., 2012](#)], whereas the atmospheric sensible heat transport is calculated without the reference temperature in the absolute temperature scale [[Hofsteenge et al., 2022](#); [Latonin et al., 2022b](#); [Overland et al., 1996](#)]. Although the mutual variability and trends might not be seriously affected, this makes it difficult to compare the absolute values of heat fluxes in the ocean and atmosphere. However, in this study, we adhere to this classical approach by choosing the reference temperature of -1.8°C for the calculation of oceanic heat transport. Thus, this study aims at comparing the variability of the oceanic and atmospheric heat fluxes of the latest decades and at evaluating their evolution in a possible future climate derived from the best Coupled Model Intercomparison Project phase 6 (CMIP6) models in the historical simulations.

2. Data and Methods

2.1. Calculation of meridional heat transport in the Atlantic Water column and in the lower troposphere

First, meridional oceanic and atmospheric heat fluxes were calculated using the datasets from the Ocean ReAnalysis System 4 (ORAS4) and European Centre for Medium-Range Weather Forecasts Reanalysis version 5 (ERA5) reanalyses [[Balmaseda et al., 2012](#); [Hersbach et al., 2020](#)]. These time series obtained were considered as the benchmarks for comparison with CMIP6 models. The oceanic reanalysis ORAS4 is one of the longest reanalyses for the ocean (along with ORAS5). This allows studying low-frequency climate variability, which is highly relevant for oceanic processes. It is available from 1958 to 2017 on a horizontal $1^{\circ} \times 1^{\circ}$ grid at 42 vertical levels. The underlying ocean model is NEMO v3.0. The atmospheric reanalysis ERA5 is a high-resolution dataset including many essential climate variables. It has recently been extended back until 1940, which makes this reanalysis one of the longest for the atmospheric and surface variables. The data is available on a horizontal $0.25^{\circ} \times 0.25^{\circ}$ grid at 137 vertical levels. The Integrated Forecasting System Cy41r2 is used as an underlying numerical weather prediction system.

From the website of ORAS4 reanalysis, two variables with monthly temporal resolution were used: seawater potential temperature and meridional current velocity at the different depths within the Atlantic Water layer. The following variables with 6-hourly temporal resolution were analyzed from the archive of the ERA5 reanalysis: air temperature, specific humidity, meridional wind velocity and geopotential at the isobaric surfaces within the lower troposphere (850–1000 hPa). The latter variable was divided by the gravitational acceleration to convert it to the geopotential heights.

Mean annual values of oceanic and atmospheric heat fluxes were calculated according to the methodology described in [[Latonin et al., 2022a](#)], but with some minor modifications described below. [Figure 1](#) shows the study area with the sections for the calculation of heat fluxes. An explanation of the choice of these sections is given in [[Latonin et al., 2022a](#)].

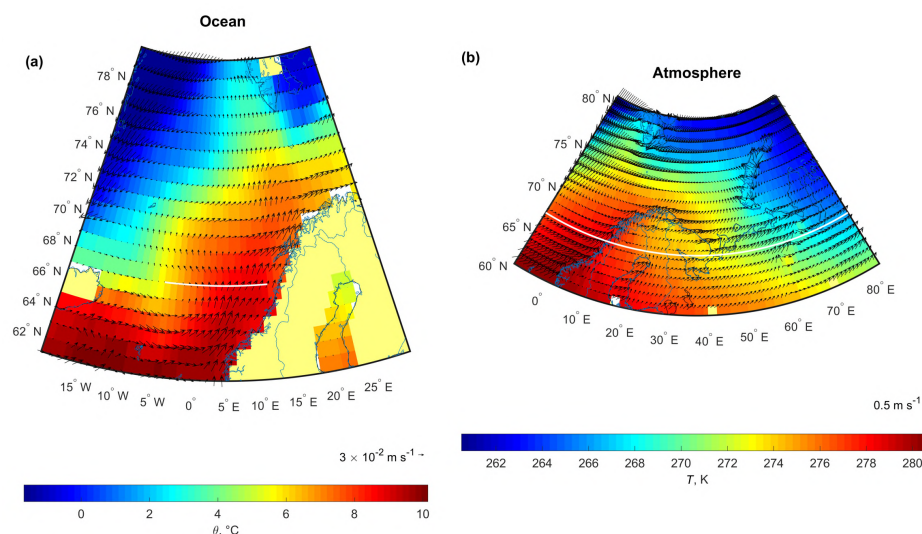


Figure 1. Average temperatures and total velocity vectors based on the ORAS4 and ERA5 reanalyses for the period 1958–2014 with monthly discreteness at a depth of 5 m in the ocean (a) and an isobaric surface of 1000 hPa in the atmosphere (b). The white lines show the sections at 66.5°N across which the heat transports were calculated.

First, the oceanic heat transport was calculated with the temperature scale in degrees Celsius using the reference temperature of -1.8°C . Second, the horizontal integration for the oceanic heat transport was carried out until 11.5°E instead of 13.5°E because the oceanic variables in the CMIP6 models usually have data until 11.5°E only. The vertical integration in the ocean was carried out down to the lower boundary of the Atlantic Water at the selected section. The boundary is taken at the isothermal of $\theta = 3^{\circ}\text{C}$. We have empirically found that its position is almost coincident to that of the isopycnal $\sigma = 27.85 \text{ kg m}^{-3}$ usually used as the limit of the water masses of Atlantic origin [Latonin et al., 2022a].

The upper boundary of the vertical integration for the atmospheric heat fluxes was changed from 800 hPa to 850 hPa. This is related to the absence of data in the CMIP6 models in the layer 800–850 hPa. In addition, the atmospheric heat fluxes were calculated from daily data, which did not affect the variability characteristics obtained using the monthly discreteness in [Latonin et al., 2022a], but made it possible to obtain more accurate absolute values of heat fluxes.

2.2. CMIP6 models analyzed in the study

Table 1 presents the list of CMIP6 models, which were used for calculations in a historical experiment for both the oceanic and atmospheric heat fluxes.

The CMIP6 models listed in Table 1 have the required parameters at similar levels as in the reanalyses, and the data cover the whole studied period 1958–2014. The number of models used for the calculation of atmospheric heat fluxes is lower than those for the oceanic heat flux. This is because many models lack data on the geopotential heights required to perform a vertical integration in the atmosphere.

The oceanic and atmospheric heat fluxes were calculated based on the CMIP6 models' data using the same specifications as in the reanalyses ORAS4 and ERA5 described in the subsection 2.1. After that, the models have been verified against the reanalyses for the historical period.

2.3. Selection of the scenarios used for the climate projections

For the climate projections in the 21st century, we used all available scenarios from the Shared Socioeconomic Pathways, i.e., from the low-end SSP119 scenario to the high-end SSP585 scenario [Riahi et al., 2017]. The creation of these scenarios, which also

take into account the socio-economic development of humanity, is one of the novelties implemented in the latest CMIP6 experimental design [Eyring *et al.*, 2016]. As in the historical simulations, here we also used the first realizations of the projected parameters needed to calculate the poleward transports of oceanic and atmospheric heat.

Table 1. A complete list of the 17 CMIP6 models in the historical experiment for the first ensemble member (r1i1p1f1). The bold font highlights the models used for the calculation of **oceanic heat transport**, whereas the bold and italic font indicates the models selected for the **oceanic and atmospheric heat transports**. Only the models covering consistent data for both flux calculations are used in our study

| No. | Name of the CMIP6 Model | Atmospheric Model | Oceanic Model | Reference |
|-----|-------------------------|-------------------|---------------|---|
| 1 | ACCESS-ESM1-5 | HadGAM2 | ACCESS-OM2 | [Ziehn <i>et al.</i> , 2019] |
| 2 | BCC-CSM2-MR | BCC_AGCM3_MR | MOM4 | [Wu <i>et al.</i> , 2018] |
| 3 | CAMS-CSM1-0 | ECHAM5_CAMS | MOM4 | [Rong, 2019] |
| 4 | CMCC-CM2-SR5 | CAM5.3 | NEMO3.6 | [Lovato and Peano, 2020] |
| 5 | CMCC-ESM2 | CAM5.3 | NEMO3.6 | [Lovato <i>et al.</i> , 2021] |
| 6 | <i>EC-Earth3</i> | IFS cy36r4 | NEMO3.6 | [EC-Earth Consortium (EC-Earth), 2019a] |
| 7 | EC-Earth3-Veg | IFS cy36r4 | NEMO3.6 | [EC-Earth Consortium (EC-Earth), 2019b] |
| 8 | EC-Earth3-Veg-LR | IFS cy36r4 | NEMO3.6 | [EC-Earth Consortium (EC-Earth), 2020] |
| 9 | <i>FGOALS-f3-L</i> | FAMIL2.2 | LICOM3.0 | [Yu, 2019] |
| 10 | <i>FGOALS-g3</i> | GAMIL3 | LICOM3.0 | [Li, 2019] |
| 11 | INM-CM4-8 | INM-AM4-8 | INM-OM5 | [Volodin <i>et al.</i> , 2019a] |
| 12 | INM-CM5-0 | INM-AM5-0 | INM-OM5 | [Volodin <i>et al.</i> , 2019b] |
| 13 | IPSL-CM6A-LR | LMDZ | NEMO-OPA | [Boucher <i>et al.</i> , 2018] |
| 14 | MPI-ESM1-2-HR | ECHAM6.3 | MPIOM1.63 | [Jungclauss <i>et al.</i> , 2019] |
| 15 | MPI-ESM1-2-LR | ECHAM6.3 | MPIOM1.63 | [Wieners <i>et al.</i> , 2019] |
| 16 | MRI-ESM2-0 | MRI-AGCM3.5 | MRI.COM4.4 | [Yukimoto <i>et al.</i> , 2019] |
| 17 | NESM3 | ECHAM v6.3 | NEMO v3.4 | [Cao and Wang, 2019] |

2.4. Selection of the sub-ensembles of CMIP6 models that most realistically simulate the meridional heat fluxes into the Atlantic sector of the Arctic

The best sub-ensembles of CMIP6 models were selected based on the ranking approach proposed in [Gnaniuk *et al.*, 2020]. This method shows better results compared to other frequently used methods for estimating and selecting a sub-ensemble of climate models.

As the data were analyzed for the study layers (without spatial data), the method for model estimation was applied in a simplified form. Interannual variability of model parameters was compared to reanalyses based on the correlation coefficient (R), root-mean-square error (RMSE), standard deviation (STD), climate prediction index (CPI) [Agosta *et al.*, 2015], trends (Tr) and biases (B_m , B_a). In order to compare the models for all these statistical metrics together, a score from 0 to 3 was assigned for each statistical metric value according to the approach. Specifically, the score was assigned based on falling into a certain percentile threshold from the total range of values for each metric: 0–25% is a score 3, 25–50% is a score 2, 50–75% is a score 1, 75–100% is a score 0. For correlation, it is vice versa. Then, total skill score was calculated for each model by summing the scores for all statistical metrics. The top 25% of considered CMIP6 models were selected as a skillful sub-ensemble based on the obtained total skill score.

The statistical metrics were calculated using the following formulas:

1. Root-mean-square deviation (RMSD):

$$\text{RMSD} = \sqrt{\frac{\sum_{i=1}^n (P_{m_i} - P_{o_i})^2}{n}},$$

where P_{m_i} is a parameter value of model data and P_{o_i} is a parameter value of reanalysis data at i time step, n is the number of time steps.

2. Correlation coefficient (R):

$$R = \frac{\frac{1}{n} \sum_{i=1}^n (P_{o_i} - \bar{P}_o) \cdot (P_{m_i} - \bar{P}_m)}{\text{STD}_o \cdot \text{STD}_m},$$

where P_{m_i} is a parameter value of model data and P_{o_i} is a parameter value of reanalysis data at i time step, \bar{P}_m is an average parameter value of model data, \bar{P}_o is an average parameter value of reanalysis data, n is the number of time steps, STD_m is a standard deviation of model data and STD_o is a standard deviation of reanalysis.

3. Standard deviation (STD) was calculated as follows:

$$\text{STD} = \sqrt{\frac{\sum_{i=1}^n (P_i - \bar{P})^2}{n-1}},$$

where P_i is a parameter value at i time step, \bar{P} is a mean parameter value, and n is the number of time steps.

4. Climate prediction index (CPI):

$$\text{CPI} = \frac{\text{RMSD}}{\text{STD}_o},$$

where RMSD is a root-mean-square deviation between model and observational data, STD_o is a standard deviation of observations.

5. dif_std is the difference between standard deviation of model data and standard deviation of reanalysis:

$$\text{dif_std} = |\text{STD}_m - \text{STD}_o|. \quad (1)$$

6. Tr_m is a difference of trends (model trend minus reanalysis trend). It is calculated as follows:

$$\text{Tr}_m = |\text{Tr}_{\text{model}} - \text{Tr}_{\text{observation}}|,$$

where Tr is a trend value of model and observational time series.

7. B_m is a mean bias (model minus reanalysis for all time steps):

$$B_m = |\overline{P_{m_i} - P_{o_i}}|,$$

where P_m and P_o are the parameter values of model and observational data accordingly at i time step.

8. B_a is an amplitude of biases (differences between model and reanalysis data for each time step):

$$B_a = |\max(P_{m_i} - P_{o_i}) - \min(P_{m_i} - P_{o_i})|,$$

where P_{m_i} and P_{o_i} are the parameter values of model and observational data accordingly, max is a maximum value, and min is a minimum value of all time steps.

3. Results

3.1. Oceanic and atmospheric heat transport in the reanalyses and in the historical simulations of the CMIP6 models. Verification of CMIP6 models and selection of the best sub-ensembles

Figure 2 shows the calculated time series of integral oceanic heat fluxes in each CMIP6 model and ORAS4 reanalysis. In addition, Figure A1 shows the oceanic heat transport in the ORAS4 reanalysis calculated using the classical approach with a reference temperature (as in Figure 2 for the red curve) and using the absolute temperature scale without a reference temperature. The correlation coefficient between the blue and orange curves in Figure A1 is 0.95. The ensemble average was calculated from the heat fluxes estimated in the individual models. This is a more accurate way than averaging the data fields in the models before calculating the heat flux [Smith et al., 2019].

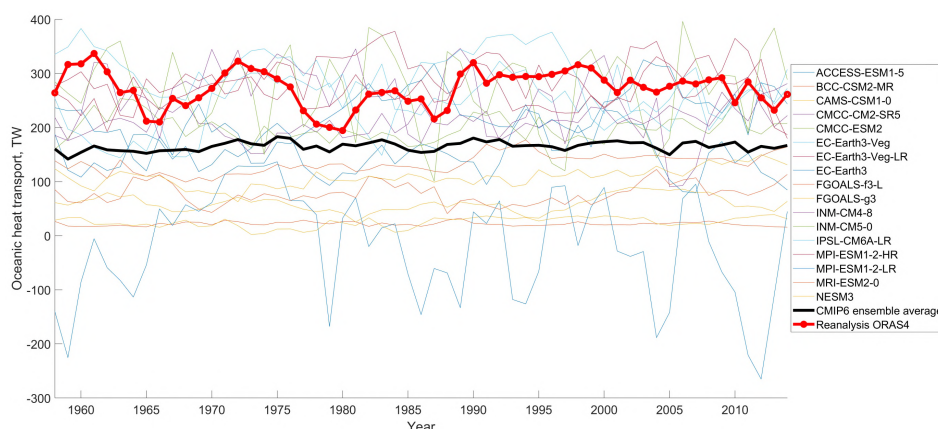


Figure 2. Time series of oceanic heat transport at the entrance to the Atlantic sector of the Arctic (along 66.5°N, between 4.5°W and 11.5°E) based on the ORAS4 reanalysis and CMIP6 models in the historical simulations. 1 TW = 10^{12} W.

The ensemble average curve in Figure 2 indicates that most CMIP6 models underestimate the value of the oceanic heat flux obtained from the ORAS4 reanalysis. Also, the nature of the interannual variability is reproduced by the CMIP6 models very inaccurately (the correlation coefficient between the CMIP6 ensemble average and the reanalysis ORAS4 is 0.26). Moreover, one of the models (MPI-ESM1-2-LR) shows unrealistic negative values of oceanic heat transport of Atlantic water into the Nordic Seas.

Statistical characteristics for assessing the quality of individual models are presented in Table 2. Based on these results, a sub-ensemble of the skillful models was selected according to the methodology described in subsection 2.4.

The results of the calculations indicate the poor quality of the CMIP6 models in simulating the oceanic heat fluxes into the Arctic. Nevertheless, for climate projections based on the SSP scenarios, a sub-ensemble was selected consisting of the four statistically best models: MPI-ESM1-2-HR, EC-Earth3-Veg-LR, CMCC-CM2-SR5, and CMCC-ESM2.

In Figure 3, the calculated time series of integral atmospheric sensible heat fluxes in each CMIP6 model and ERA5 reanalysis are shown. As for the oceanic heat flux, the ensemble average was found from the heat fluxes calculated in the individual models.

Similarly to the results with the oceanic heat flux, most CMIP6 models underestimate the atmospheric sensible heat flux that is derived from the ERA5 reanalysis. This is also reflected in the ensemble average (black curve). In addition, the interannual variability is reproduced very poorly by the CMIP6 historical simulations (the correlation coefficient between the CMIP6 ensemble average and the reanalysis ERA5 is -0.07). Table 3 presents statistical characteristics for assessing the quality of individual models relative to the reanalysis for the past period.

The calculation results confirm the poor quality of the CMIP6 models in reproducing the atmospheric sensible heat fluxes into the Arctic. For climate projections under the SSP scenarios, a sub-ensemble was selected from the two models with the best correlation to the reanalysis: INM-CM4-8 and INM-CM5-0.

Table 2. Statistical characteristics used for the evaluation of the quality of CMIP6 models in reproducing the oceanic heat transport relative to the ORAS4 reanalysis. The bold font highlights the four models selected to be used in the climate projection studies. The dimension of RMSD and dif_std is TW, and the dimension of Tr_m is $TW\ yr^{-1}$, of B_m is TW and of B_a is TW, respectively.

| No. | Models | RMSD | | R | | CPI | | dif_std | | Tr _m | | B _m | | B _a | | Total score |
|-----|------------------|--------|------|-------|------|------|-------|---------|------|-----------------|--------|----------------|--------|----------------|---|-------------|
| 1 | ACCESS-ESM1-5 | 129.10 | 2 | 0.19 | 0 | 3.90 | 2 | 5.70 | 3 | 0.11 | 3 | 120.50 | 2 | 185.10 | 2 | 14 |
| 2 | BCC-CSM2-MR | 252.60 | 0 | −0.10 | 0 | 7.60 | 0 | 29.80 | 2 | 0.09 | 3 | 250.30 | 0 | 151.10 | 3 | 8 |
| 3 | CAMS-CSM1-0 | 249.40 | 0 | 0.15 | 0 | 7.50 | 0 | 24.10 | 2 | 0.15 | 3 | 247.10 | 0 | 145.20 | 3 | 8 |
| 4 | CMCC-CM2-SR5 | 77.10 | 2 | −0.15 | 0 | 2.30 | 2 | 8.50 | 3 | 0.63 | 2 | 62.80 | 3 | 184.80 | 3 | 15 |
| 5 | CMCC-ESM2 | 83.50 | 2 | 0.06 | 0 | 2.50 | 2 | 11.00 | 3 | 0.13 | 3 | 73.70 | 2 | 170.70 | 3 | 15 |
| 6 | EC-Earth3-Veg | 63.50 | 3 | 0.06 | 0 | 1.90 | 3 | 14.60 | 3 | 1.02 | 1 | 28.30 | 3 | 255.60 | 1 | 14 |
| 7 | EC-Earth3-Veg-LR | 58.80 | 3 | −0.05 | 0 | 1.80 | 3 | 7.90 | 3 | 0.00 | 3 | 22.10 | 3 | 208.10 | 2 | 17 |
| 8 | EC-Earth3 | 78.60 | 2 | −0.21 | 0 | 2.30 | 2 | 13.20 | 3 | 1.37 | 0 | 47.30 | 3 | 276.90 | 1 | 11 |
| 9 | FGOALS-f3-L | 142.80 | 1 | 0.23 | 0 | 4.30 | 1 | 16.10 | 3 | 0.61 | 2 | 138.70 | 2 | 149.80 | 3 | 12 |
| 10 | FGOALS-g3 | 214.80 | 0 | 0.35 | 1 | 6.40 | 0 | 18.70 | 2 | 0.08 | 3 | 212.50 | 1 | 116.90 | 3 | 10 |
| 11 | INM-CM4-8 | 72.20 | 2 | 0.01 | 0 | 2.20 | 2 | 27.70 | 2 | 1.18 | 0 | 19.40 | 3 | 306.00 | 1 | 10 |
| 12 | INM-CM5-0 | 76.80 | 2 | 0.07 | 0 | 2.30 | 2 | 37.80 | 1 | 0.15 | 3 | 1.20 | 3 | 336.40 | 0 | 11 |
| 13 | IPSL-CM6A-LR | 57.30 | 3 | 0.33 | 1 | 1.70 | 3 | 21.40 | 2 | 1.16 | 0 | 18.80 | 3 | 234.90 | 2 | 14 |
| 14 | MPI-ESM1-2-HR | 45.20 | 3 | 0.10 | 0 | 1.40 | 3 | 0.20 | 3 | 0.41 | 2 | 6.60 | 3 | 182.10 | 3 | 17 |
| 15 | MPI-ESM1-2-LR | 308.60 | 0 | 0.14 | 0 | 9.20 | 0 | 65.80 | 0 | 1.08 | 0 | 291.90 | 0 | 388.60 | 0 | 0 |
| 16 | MRI-ESM2-0 | 199.20 | 0 | −0.32 | 0 | 6.00 | 0 | 14.30 | 3 | 0.15 | 3 | 194.40 | 1 | 161.40 | 3 | 10 |
| 17 | NESM3 | 169.00 | 1 | −0.19 | 0 | 5.10 | 1 | 15.90 | 3 | 0.60 | 2 | 164.10 | 1 | 171.80 | 3 | 11 |
| max | | 308.60 | 1.00 | | 9.20 | | 65.80 | | 1.37 | | 291.90 | | 388.60 | | | |
| 75% | | 197.50 | 0.75 | | 5.90 | | 49.20 | | 1.02 | | 218.00 | | 320.70 | | | |
| 50% | | 131.70 | 0.50 | | 3.90 | | 32.80 | | 0.68 | | 145.30 | | 252.70 | | | |
| 25% | | 65.80 | 0.25 | | 2.00 | | 16.40 | | 0.34 | | 72.70 | | 184.80 | | | |
| min | | 45.20 | 0.00 | | 1.40 | | 0.20 | | 0.00 | | 1.20 | | 116.90 | | | |

very good

satisfactory

unsatisfactory

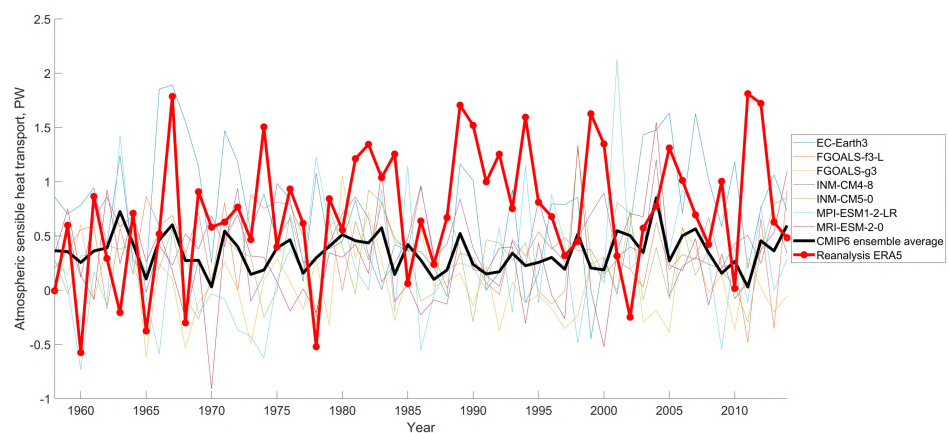


Figure 3. Time series of atmospheric sensible heat transport at the entrance to the Atlantic sector of the Arctic (along 66.5°N, between 5°W and 80°E) using the ERA5 reanalysis and CMIP6 models in the historical experiment. 1 PW = 10^{15} W.

Table 3. Statistical characteristics used for the evaluation of the quality of CMIP6 models in the reproduction of the atmospheric sensible heat transport relative to the ERA5 reanalysis. The bold font highlights the two models selected to be used in the climate projection studies. The dimension of RMSD and dif_std is PW, and the dimension of Tr_m is $PW\ yr^{-1}$, of B_m is PW and of B_a is PW, respectively.

| No. | Models | RMSD | | R | | CPI | | dif_std | | Trm | | Bm | | Ba | | Total score |
|-----|---------------|------|------|-------|-----|-----|------|---------|-------|-------|------|------|-----|-----|---|-------------|
| 1 | EC-Earth3 | 0.83 | 1 | −0.11 | 0 | 1.4 | 1 | 0.06 | 3 | 0.012 | 0 | 0.01 | 3 | 3.9 | 0 | 8 |
| 2 | FGOALS-f3-L | 0.75 | 3 | −0.01 | 0 | 1.3 | 3 | 0.26 | 0 | 0.015 | 0 | 0.34 | 1 | 3.5 | 1 | 8 |
| 3 | FGOALS-g3 | 0.93 | 0 | −0.02 | 0 | 1.6 | 0 | 0.24 | 0 | 0.014 | 0 | 0.64 | 0 | 2.9 | 2 | 2 |
| 4 | INM-CM4-8 | 0.69 | 3 | 0.09 | 0 | 1.2 | 3 | 0.29 | 0 | 0.011 | 1 | 0.27 | 2 | 2.4 | 3 | 12 |
| 5 | INM-CM5-0 | 0.8 | 2 | 0 | 0 | 1.4 | 2 | 0.24 | 0 | 0.008 | 2 | 0.43 | 1 | 3.1 | 2 | 9 |
| 6 | MPI-ESM1-2-LR | 0.95 | 0 | −0.07 | 0 | 1.6 | 0 | 0.04 | 3 | 0.004 | 3 | 0.46 | 1 | 3.9 | 0 | 7 |
| 7 | MRI-ESM2-0 | 0.86 | 1 | −0.01 | 0 | 1.5 | 1 | 0.15 | 1 | 0.008 | 2 | 0.45 | 1 | 2.9 | 2 | 8 |
| max | | 0.95 | 1 | | 1.6 | | 0.29 | | 0.015 | | 0.64 | | 3.9 | | | |
| 75% | | 0.88 | 0.75 | | 1.5 | | 0.19 | | 0.012 | | 0.47 | | 3.5 | | | |
| 50% | | 0.82 | 0.5 | | 1.4 | | 0.13 | | 0.009 | | 0.31 | | 3.2 | | | |
| 25% | | 0.75 | 0.25 | | 1.3 | | 0.06 | | 0.006 | | 0.16 | | 2.8 | | | |
| min | | 0.69 | 0 | | 1.2 | | 0.04 | | 0.004 | | 0.01 | | 2.4 | | | |

very good

satisfactory

unsatisfactory

In **Figure 4**, the calculated time series of integral atmospheric latent heat fluxes in each CMIP6 model and ERA5 reanalysis are shown.

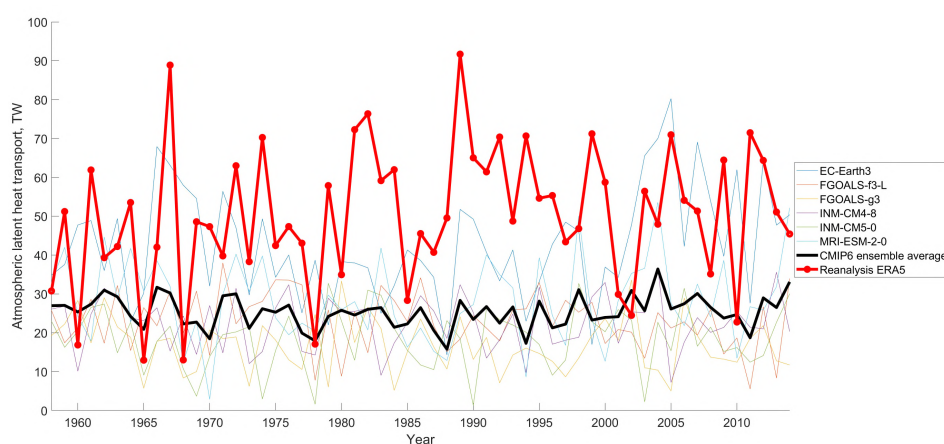


Figure 4. Time series of atmospheric latent heat transport at the entrance to the Atlantic sector of the Arctic (along 66.5°N, between 5°W and 80°E) for the ERA5 reanalysis and CMIP6 models in the historical experiment. 1 TW = 10^{12} W.

The curves in **Figure 4** clearly show that CMIP6 models strongly underestimate the magnitude of the atmospheric latent heat transport obtained from the ERA5 reanalysis. The interannual variability is also poorly reproduced by the climate models compared to the reanalysis (the correlation coefficient between the CMIP6 ensemble average and the reanalysis ERA5 is 0.08).

Table 4 presents statistical characteristics for assessing the correlations of individual models with the reanalysis for the past period.

The results in **Table 4** confirm the poor quality of the CMIP6 models in reproducing the atmospheric latent heat fluxes into the Arctic. For the assessment of the climate

projections, under the SSP scenarios, a sub-ensemble was selected from the two statistically best performing models: EC-Earth3 and MRI-ESM2-0.

Table 4. Statistical characteristics used for the evaluation of the quality of CMIP6 models in the reproduction of the atmospheric latent heat transport relative to the ERA5 reanalysis. The bold font highlights the two models selected to be used in the climate projection studies. The dimension of RMSD and dif_std is TW, and the dimension of Tr_m is TW yr^{-1} , of B_m is TW and of B_a is TW, respectively.

| No. | Models | RMSD | | R | | CPI | | dif_std | | Trm | | Bm | | Ba | | Total score | |
|-----|-------------|-----------|---|-------|---|--------------|---|---------|---|----------------|---|-------|---|-------|---|-------------|--|
| 1 | EC-Earth3 | 23.70 | 3 | −0.01 | 0 | 1.40 | 3 | 3.50 | 3 | 0.05 | 3 | 7.40 | 3 | 99.20 | 0 | 15 | |
| 2 | FGOALS-f3-L | 33.00 | 1 | 0.02 | 0 | 1.90 | 1 | 10.20 | 0 | 0.31 | 0 | 27.10 | 0 | 86.80 | 2 | 4 | |
| 3 | FGOALS-g3 | 38.40 | 0 | −0.02 | 0 | 2.20 | 0 | 10.60 | 0 | 0.28 | 0 | 33.40 | 0 | 81.70 | 3 | 3 | |
| 4 | INM-CM4-8 | 33.50 | 1 | 0.01 | 0 | 1.90 | 1 | 10.60 | 0 | 0.22 | 1 | 27.70 | 0 | 84.90 | 2 | 5 | |
| 5 | INM-CM5-0 | 36.70 | 0 | 0.11 | 0 | 2.10 | 0 | 9.70 | 0 | 0.19 | 1 | 31.70 | 0 | 76.80 | 3 | 4 | |
| 6 | MRI-ESM2-0 | 29.30 | 2 | 0.11 | 0 | 1.70 | 2 | 6.80 | 2 | 0.19 | 1 | 21.90 | 1 | 84.50 | 2 | 10 | |
| max | | 38.40 | | 1.00 | | 2.20 | | 10.60 | | 0.31 | | 33.40 | | 99.20 | | | |
| 75% | | 34.70 | | 0.75 | | 2.00 | | 8.80 | | 0.24 | | 26.90 | | 93.60 | | | |
| 50% | | 31.00 | | 0.50 | | 1.80 | | 7.10 | | 0.18 | | 20.40 | | 88.00 | | | |
| 25% | | 27.40 | | 0.25 | | 1.60 | | 5.30 | | 0.11 | | 13.90 | | 82.40 | | | |
| min | | 23.70 | | 0.00 | | 1.40 | | 3.50 | | 0.05 | | 7.40 | | 76.80 | | | |
| | | very good | | | | satisfactory | | | | unsatisfactory | | | | | | | |

3.2. Climate projections of oceanic and atmospheric heat transport until 2100

The interannual variability of oceanic heat transport into the Arctic is presented in [Figure 5](#) for the reanalysis ORAS4, CMIP6 historical simulations and five different climate scenarios. The main statistical characteristics for the comparison are given in [Table 5](#).

Figure 5 and Table 5 show that, with the exception of the SSP119 scenario, the future climate of the Arctic is characterized by a significantly increased oceanic heat transport into the Arctic Ocean relative to the past historical period. The interannual variability of the oceanic heat flux in all the future SSP scenarios is also significantly higher than during the historical period. In each of the future scenarios, the linear trends of the oceanic heat flux are positive and statistically significant, with a minimum of 0.6 TW yr^{-1} in the SSP119 scenario and a maximum of 3.3 TW yr^{-1} in the SSP585 scenario, reflecting the climate development in the scenarios studied. The CMIP6 historical simulations also reveal a statistically significant linear increasing trend, but its magnitude is only 0.3 TW yr^{-1} . The oceanic heat transport scenarios are highly coherent and robust: between all pairs of time series, the correlation coefficients are positive and statistically significant, and for the SSP126–SSP585 scenarios, the correlation coefficients are always higher than 0.8.

Figure 6 presents the interannual variability of atmospheric sensible heat transport into the Arctic for the reanalysis ERA5, CMIP6 historical simulations and four different climate scenarios. The corresponding statistical characteristics for the comparison are presented in Table 6.

It is clearly seen from [Figure 6](#) and [Table 6](#) that in the future climate of the Arctic, the order of magnitude and the scale of variability of atmospheric sensible heat transport will remain approximately at the same level as in the historical period, for all future climate development scenarios. However, the mean values steadily increase from the SSP126 scenario to the SSP585 scenario. The pattern of variability from scenario to scenario is unstable: the standard deviations irregularly increase and decrease from one scenario

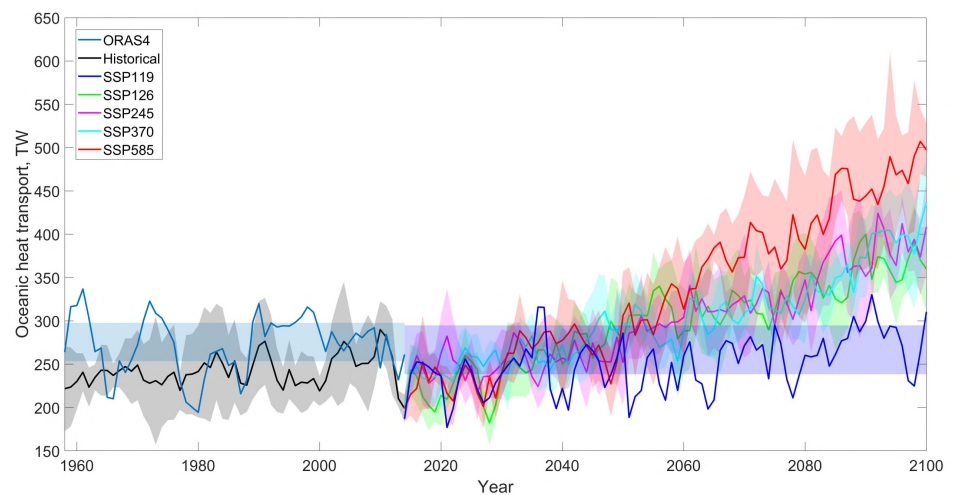


Figure 5. Interannual variability of the oceanic heat transport into the Arctic (TW) according to the ORAS4 reanalysis and the sub-ensemble average of four selected CMIP6 climate models (MPI-ESM1-2-HR, EC-Earth3-Veg-LR, CMCC-CM2-SR5, and CMCC-ESM2) in the historical period (1958–2014) and their climate simulations for five development scenarios (SSP119, SSP126, SSP245, SSP370, and SSP585) for the period 2015–2100. Uncertainty, calculated as the interquartile range (difference between the 75th and 25th percentiles of the data), is highlighted in solid; in the case of one time series (the ORAS4 reanalysis and the SSP119 scenario), such uncertainty is constant. The SSP119 scenario is only available for the EC-Earth3-Veg-LR model. $1 \text{ TW} = 10^{12} \text{ W}$.

Table 5. Statistical characteristics of the time series of the oceanic heat transport displayed in Figure 5. Std is the standard deviation (TW) and k is the slope of the linear trend (TW yr^{-1}). The values in bold denote statistically significant linear trends at the 5% significance level. The uncertainties of the mean values are based on the standard errors and are calculated for the 5% significance level. $1 \text{ TW} = 10^{12} \text{ W}$.

| | Mean (TW) | Std (TW) | k (TW yr^{-1}) |
|------------|--------------|----------|-----------------------------|
| Historical | 242 ± 5 | 18 | 0.3 |
| SSP119 | 252 ± 7 | 32 | 0.6 |
| SSP126 | 297 ± 11 | 51 | 1.9 |
| SSP245 | 302 ± 11 | 53 | 1.9 |
| SSP370 | 303 ± 11 | 51 | 1.9 |
| SSP585 | 336 ± 19 | 86 | 3.3 |

Table 6. Statistical characteristics of the time series of the atmospheric sensible heat transport displayed in Figure 6. Std is the standard deviation (TW) and k is the slope of the linear trend (TW yr^{-1}). The values in bold denote statistically significant linear trends at the 5% significance level. The uncertainties of the mean values are based on the standard errors and are calculated for the 5% significance level. $1 \text{ TW} = 10^{12} \text{ W}$.

| | Mean (TW) | Std (TW) | k (TW yr^{-1}) |
|------------|--------------|----------|-----------------------------|
| Historical | 370 ± 60 | 230 | 0.6 |
| SSP126 | 320 ± 60 | 260 | −2 |
| SSP245 | 430 ± 60 | 290 | 2 |
| SSP370 | 440 ± 60 | 270 | 3 |
| SSP585 | 460 ± 50 | 250 | 3 |

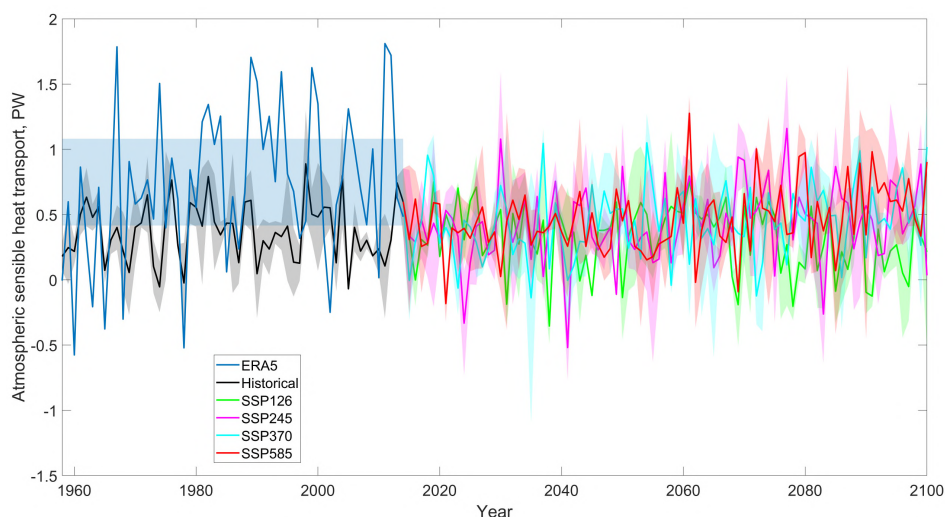


Figure 6. Interannual variability of the atmospheric sensible heat transport into the Arctic (PW) according to the ERA5 reanalysis and the sub-ensemble average of two selected CMIP6 climate models (INM-CM4-8 and INM-CM5-0) in the historical period (1958–2014) and their climate simulations for four development scenarios (SSP126, SSP245, SSP370, and SSP585) for the period 2015–2100. Uncertainty, calculated as the interquartile range (difference between the 75th and 25th percentiles of the data), is highlighted in solid; in the case of one time series (the ERA5 reanalysis), such uncertainty is constant. Positive values correspond to the northward flux direction. $1 \text{ PW} = 10^{15} \text{ W}$.

to another. In the historical period, there is a very weak positive trend, whereas for the SSP126 future scenario the linear trend is negative. Starting from the SSP245 scenario, the trends are always positive, with the statistically significant maximum values of 3 TW in the SSP370 and SSP585 scenarios. Correlation analysis showed that the scenarios are weakly interconnected because there are no statistically significant correlation coefficients among the scenarios. This stands in contrast to the highly correlated scenarios of oceanic heat transport discussed above and shown in Figure 5.

The interannual variability of atmospheric latent heat transport into the Arctic for the reanalysis ERA5, CMIP6 historical simulations and five different climate scenarios are presented in Figure 7. Table 7 summarizes the respective statistical characteristics.

Table 7. Statistical characteristics of the time series of the atmospheric latent heat transport displayed in Figure 7. Std is the standard deviation (TW) and k is the slope of the linear trend (TW yr^{-1}). The values in bold denote statistically significant linear trends at the 5% significance level. The uncertainties of the mean values are based on the standard errors and are calculated for the 5% significance level. $1 \text{ TW} = 10^{12} \text{ W}$.

| | Mean (TW) | Std (TW) | k (TW yr^{-1}) |
|------------|------------|----------|-----------------------------|
| Historical | 36 ± 3 | 10 | 0.1 |
| SSP119 | 30 ± 2 | 12 | −0.1 |
| SSP126 | 39 ± 2 | 10 | 0.03 |
| SSP245 | 41 ± 3 | 12 | 0.1 |
| SSP370 | 43 ± 3 | 13 | 0.2 |
| SSP585 | 47 ± 3 | 15 | 0.3 |

The results for the atmospheric latent heat transport in Figure 7 are similar to those shown in Figure 6 for the atmospheric sensible heat transport; however, there are some important differences. The mean annual values in the scenarios SSP119–SSP585 are significantly lower than for the sensible heat transport, but the steady increase from the low-end to the high-end climate scenarios is preserved (Table 7). According to the

standard deviations in Table 7, the irregular changes in the variability are present too. The slopes of the linear trends increase from the low-end to the high-end climate scenarios, and two positive trends are statistically significant for the SSP370 and SSP585 scenarios. Thus, for the atmospheric latent heat transport, the trend of increase is stronger than for the atmospheric sensible heat transport from 2015 to 2100. There are few statistically significant correlation coefficients: 0.26 between the SSP370 and SSP585 scenarios and -0.23 between the SSP126 and SSP245 scenarios.

For all climate development scenarios, the components of atmospheric heat transport in the selected models are not correlated with each other. This is expected given different models identified for the sensible and latent heat transport components.

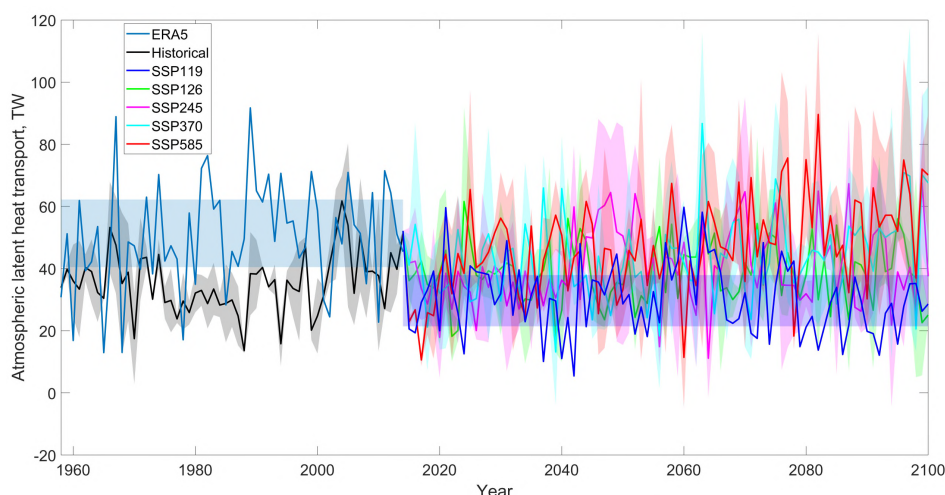


Figure 7. Interannual variability of the atmospheric latent heat transport into the Arctic (TW) according to the ERA5 reanalysis and the sub-ensemble average of two selected climate models CMIP6 (EC-Earth3 and MRI-ESM2-0) in the historical period (1958–2014) and their climate simulations for five development scenarios for the period 2015–2100. Uncertainty, calculated as the interquartile range (difference between the 75th and 25th percentiles of the data), is highlighted in solid; in the case of one time series (the ERA5 reanalysis and the SSP119 scenario), such uncertainty is constant. The SSP119 scenario is only available for the MRI-ESM2-0 model. Positive values correspond to the northward flux direction. $1 \text{ TW} = 10^{12} \text{ W}$.

4. Discussion and Conclusions

One of the main findings of this study is a poor quality of the state-of-the-art CMIP6 climate models in simulating the meridional oceanic and atmospheric heat fluxes at the entrance to the Atlantic sector of the Arctic. We have shown that for the studied sections, the transports of oceanic and atmospheric heat into the Atlantic sector of the Arctic are not comparable in magnitude. During the period 1958–2014, the mean annual values of oceanic heat transport obtained from the ORAS4 ocean reanalysis and of the atmospheric sensible heat transport from the ERA5 atmospheric reanalysis are $272 \pm 9 \text{ TW}$ and $720 \pm 160 \text{ TW}$, respectively. An additional transport of atmospheric latent heat of $50 \pm 5 \text{ TW}$ formally indicates that, over the past historical period, the atmosphere transports more heat to the Arctic than the ocean. However, our estimations are obtained along a limited transect at 66.5°N without considering the total heat budget. This means the absolute values of heat fluxes in the ocean and atmosphere cannot be compared due to different temperature scales and reference temperatures in the equations. If the equivalent equations and the same absolute temperature scale are used for the estimation of the advective sensible heat fluxes in the ocean and atmosphere, the ocean transports more heat than the atmosphere [Latónin *et al.*, 2022a]. At the same time, the variability patterns are almost not affected depending on the method used (see also Figure A1).

Validation procedure, using the independent ORAS4 and ERA5 reanalyses, allows choosing the statistically best performing CMIP6 models to project the relative role of the heat transports in respectively the ocean and atmosphere, by the end of the 21st century. We note that the ocean blocks in three of the four selected CMIP6 models (CMCC-CM2-SR5, CMCC-ESM2 and EC-Earth3-Veg-LR models) are based on the NEMO ocean model. It has recently been documented that the projected Arctic climate change will be intensified in the cluster of the NEMO-based models in CMIP6 [Pan *et al.*, 2023]. Based on our analysis, the best performing model for the atmospheric latent heat transport is the EC-Earth3 model. This means that the family of EC-Earth3 models is statistically best in the simulation of both the oceanic heat transport and atmospheric latent heat transport. This could be expected since EC-Earth3 models use the same type of oceanic and atmospheric models as the ORAS4 and ERA5 reanalyses used here for validation of performance of the CMIP6 models. Nevertheless, even the best performing model and the means of the best sub-ensembles of the models, do not reproduce the interannual variability obtained from the reanalyses. This might be related to a common problem of climate models with simulating the internal variability adequately [Kravtsov *et al.*, 2018].

According to our results, independent on the predicted climate scenario, the increase of the meridional oceanic heat transport into the Arctic Ocean in the 21st century will be dominant over the increase of the atmospheric heat transport into the Arctic. In terms of the projected trends, this is consistent with previous studies for the CMIP3 climate models' projections [Hwang *et al.*, 2011].

Acknowledgments. This study was funded by the Russian Science Foundation (RSF), grant number 23-77-01046 (<https://rscf.ru/en/project/23-77-01046/>).

Appendix A

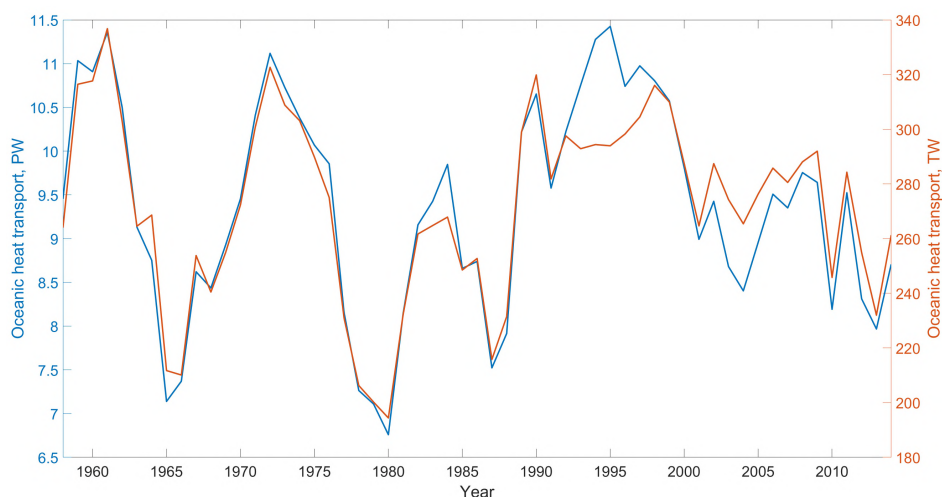


Figure A1. Time series of oceanic heat transport at the entrance to the Atlantic sector of the Arctic (along 66.5°N, between 4.5°W and 11.5°E) based on the ORAS4 reanalysis. The orange curve corresponds to the classical approach of calculation used in the main text of the article (with the subtraction of the reference temperature of -1.8°C), whereas the blue curve represents an alternative approach of calculation using the absolute temperature scale without a reference temperature. $1\text{ TW} = 10^{12}\text{ W}$ and $1\text{ PW} = 10^{15}\text{ W}$.

References

- Agosta, C., X. Fettweis, and R. Datta (2015), Evaluation of the CMIP5 models in the aim of regional modelling of the Antarctic surface mass balance, *The Cryosphere*, 9(6), 2311–2321, <https://doi.org/10.5194/tc-9-2311-2015>.
- Alexeev, V. A., J. E. Walsh, V. V. Ivanov, V. A. Semenov, and A. V. Smirnov (2017), Warming in the Nordic Seas, North Atlantic storms and thinning Arctic sea ice, *Environmental Research Letters*, 12(8), 084,011, <https://doi.org/10.1088/1748-9326/aa7a1d>.
- Balmaseda, M. A., K. Mogensen, and A. T. Weaver (2012), Evaluation of the ECMWF ocean reanalysis system ORAS4, *Quarterly Journal of the Royal Meteorological Society*, 139(674), 1132–1161, <https://doi.org/10.1002/qj.2063>.
- Bjerknes, J. (1964), *Atlantic Air-Sea Interaction*, pp. 1–82, Advances in Geophysics, Elsevier, [https://doi.org/10.1016/S0065-2687\(08\)60005-9](https://doi.org/10.1016/S0065-2687(08)60005-9).
- Boucher, O., S. Denvil, G. Levvasseur, et al. (2018), IPSL IPSL-CM6A-LR model output prepared for CMIP6 CMIP historical, <https://doi.org/10.22033/ESGF/CMIP6.5195>.
- Cao, J., and B. Wang (2019), NUIST NESMv3 model output prepared for CMIP6 CMIP historical, <https://doi.org/10.22033/ESGF/CMIP6.8769>.
- Docquier, D., and T. Koenigk (2021), A review of interactions between ocean heat transport and Arctic sea ice, *Environmental Research Letters*, 16(12), 123,002, <https://doi.org/10.1088/1748-9326/ac30be>.
- EC-Earth Consortium (EC-Earth) (2019a), EC-Earth-Consortium EC-Earth3 model output prepared for CMIP6 CMIP historical, <https://doi.org/10.22033/ESGF/CMIP6.4700>.
- EC-Earth Consortium (EC-Earth) (2019b), EC-Earth-Consortium EC-Earth3-Veg model output prepared for CMIP6 ScenarioMIP, <https://doi.org/10.22033/ESGF/CMIP6.727>.
- EC-Earth Consortium (EC-Earth) (2020), EC-Earth-Consortium EC-Earth3-Veg-LR model output prepared for CMIP6 CMIP historical, <https://doi.org/10.22033/ESGF/CMIP6.4707>.
- Esau, I., L. H. Pettersson, M. Cancet, et al. (2023), The Arctic Amplification and Its Impact: A Synthesis through Satellite Observations, *Remote Sensing*, 15(5), 1354, <https://doi.org/10.3390/rs15051354>.
- Eyring, V., S. Bony, G. A. Meehl, et al. (2016), Overview of the Coupled Model Intercomparison Project Phase 6 (CMIP6) experimental design and organization, *Geoscientific Model Development*, 9(5), 1937–1958, <https://doi.org/10.5194/gmd-9-1937-2016>.
- Gnatiuk, N., I. Radchenko, R. Davy, E. Morozov, and L. Bobylev (2020), Simulation of factors affecting *Emiliania huxleyi* blooms in Arctic and sub-Arctic seas by CMIP5 climate models: model validation and selection, *Biogeosciences*, 17(4), 1199–1212, <https://doi.org/10.5194/bg-17-1199-2020>.
- Goosse, H., J. E. Kay, K. C. Armour, et al. (2018), Quantifying climate feedbacks in polar regions, *Nature Communications*, 9(1), <https://doi.org/10.1038/s41467-018-04173-0>.
- Graham, R. M., L. Cohen, A. A. Petty, et al. (2017), Increasing frequency and duration of Arctic winter warming events, *Geophysical Research Letters*, 44(13), 6974–6983, <https://doi.org/10.1002/2017GL073395>.
- Hersbach, H., B. Bell, P. Berrisford, et al. (2020), The ERA5 global reanalysis, *Quarterly Journal of the Royal Meteorological Society*, 146(730), 1999–2049, <https://doi.org/10.1002/qj.3803>.
- Hofsteenge, M. G., R. G. Graversen, J. H. Rydsaa, and Z. Rey (2022), The impact of atmospheric Rossby waves and cyclones on the Arctic sea ice variability, *Climate Dynamics*, 59(1–2), 579–594, <https://doi.org/10.1007/s00382-022-06145-z>.
- Hwang, Y.-T., D. M. W. Frierson, and J. E. Kay (2011), Coupling between Arctic feedbacks and changes in poleward energy transport, *Geophysical Research Letters*, 38(17), <https://doi.org/10.1029/2011GL048546>.
- Jungclaus, J., M. Bittner, K.-H. Wieners, et al. (2019), MPI-M MPI-ESM1.2-HR model output prepared for CMIP6 CMIP historical, <https://doi.org/10.22033/ESGF/CMIP6.6594>.

- Koenigk, T., L. Brodeau, R. G. Graversen, et al. (2012), Arctic climate change in 21st century CMIP5 simulations with EC-Earth, *Climate Dynamics*, 40(11–12), 2719–2743, <https://doi.org/10.1007/s00382-012-1505-y>.
- Kravtsov, S., C. Grimm, and S. Gu (2018), Global-scale multidecadal variability missing in state-of-the-art climate models, *npj Climate and Atmospheric Science*, 1(1), <https://doi.org/10.1038/s41612-018-0044-6>.
- Latonin, M. M., I. L. Bashmachnikov, and L. P. Bobylev (2022a), Bjerknes compensation mechanism as a possible trigger of the low-frequency variability of Arctic amplification, *Russian Journal of Earth Sciences*, pp. 1–21, <https://doi.org/10.2205/2022ES000820>.
- Latonin, M. M., L. P. Bobylev, I. L. Bashmachnikov, and R. Davy (2022b), Dipole pattern of meridional atmospheric internal energy transport across the Arctic gate, *Scientific Reports*, 12(1), <https://doi.org/10.1038/s41598-022-06371-9>.
- Li, L. (2019), CAS FGOALS-g3 model output prepared for CMIP6 CMIP historical, <https://doi.org/10.22033/ESGF/CMIP6.3356>.
- Liang, Y., N. P. Gillett, and A. H. Monahan (2020), Climate Model Projections of 21st Century Global Warming Constrained Using the Observed Warming Trend, *Geophysical Research Letters*, 47(12), <https://doi.org/10.1029/2019GL086757>.
- Lique, C., H. L. Johnson, and Y. Plancherel (2017), Emergence of deep convection in the Arctic Ocean under a warming climate, *Climate Dynamics*, 50(9–10), 3833–3847, <https://doi.org/10.1007/s00382-017-3849-9>.
- Lovato, T., and D. Peano (2020), CMCC CMCC-CM2-SR5 model output prepared for CMIP6 CMIP historical, <https://doi.org/10.22033/ESGF/CMIP6.3825>.
- Lovato, T., D. Peano, and M. Butenschön (2021), CMCC CMCC-ESM2 model output prepared for CMIP6 CMIP historical, <https://doi.org/10.22033/ESGF/CMIP6.13195>.
- Madonna, E., and A. B. Sandø (2021), Understanding Differences in North Atlantic Poleward Ocean Heat Transport and Its Variability in Global Climate Models, *Geophysical Research Letters*, 49(1), <https://doi.org/10.1029/2021GL096683>.
- Outten, S., I. Esau, and O. H. Otterå (2018), Bjerknes Compensation in the CMIP5 Climate Models, *Journal of Climate*, 31(21), 8745–8760, <https://doi.org/10.1175/JCLI-D-18-0058.1>.
- Overland, J. E., P. Turet, and A. H. Oort (1996), Regional Variations of Moist Static Energy Flux into the Arctic, *Journal of Climate*, 9(1), 54–65, [https://doi.org/10.1175/1520-0442\(1996\)009<0054:RVOMSE>2.0.CO;2](https://doi.org/10.1175/1520-0442(1996)009<0054:RVOMSE>2.0.CO;2).
- Pan, R., Q. Shu, Q. Wang, et al. (2023), Future Arctic Climate Change in CMIP6 Strikingly Intensified by NEMO-Family Climate Models, *Geophysical Research Letters*, 50(4), <https://doi.org/10.1029/2022GL102077>.
- Polyakov, I. V., L. A. Timokhov, V. A. Alexeev, et al. (2010), Arctic Ocean Warming Contributes to Reduced Polar Ice Cap, *Journal of Physical Oceanography*, 40(12), 2743–2756, <https://doi.org/10.1175/2010JPO4339.1>.
- Riahi, K., D. P. van Vuuren, E. Kriegler, et al. (2017), The Shared Socioeconomic Pathways and their energy, land use, and greenhouse gas emissions implications: An overview, *Global Environmental Change*, 42, 153–168, <https://doi.org/10.1016/j.gloenvcha.2016.05.009>.
- Rong, X. (2019), CAMS CAMS_CSM1.0 model output prepared for CMIP6 CMIP historical, <https://doi.org/10.22033/ESGF/CMIP6.9754>.
- Serreze, M. C., and R. G. Barry (2014), *The Arctic Climate System*, Cambridge University Press, <https://doi.org/10.1017/CBO9781139583817>.
- Smith, D. M., J. A. Screen, C. Deser, et al. (2019), The Polar Amplification Model Intercomparison Project (PAMIP) contribution to CMIP6: investigating the causes and consequences of polar amplification, *Geoscientific Model Development*, 12(3), 1139–1164, <https://doi.org/10.5194/gmd-12-1139-2019>.
- van der Swaluw, E., S. S. Drijfhout, and W. Hazeleger (2007), Bjerknes Compensation at High Northern Latitudes: The Ocean Forcing the Atmosphere, *Journal of Climate*, 20(24), 6023–6032, <https://doi.org/10.1175/2007JCLI1562.1>.
- Volodin, E., E. Mortikov, A. Gritsun, et al. (2019a), INM INM-CM4-8 model output prepared for CMIP6 ScenarioMIP, <https://doi.org/10.22033/ESGF/CMIP6.12321>.

- Volodin, E., E. Mortikov, A. Gritsun, et al. (2019b), INM INM-CM5-0 model output prepared for CMIP6 CMIP historical, <https://doi.org/10.22033/ESGF/CMIP6.5070>.
- Wieners, K.-H., M. Giorgetta, J. Jungclaus, et al. (2019), MPI-M MPI-ESM1.2-LR model output prepared for CMIP6 CMIP historical, <https://doi.org/10.22033/ESGF/CMIP6.6595>.
- Wu, T., M. Chu, M. Dong, et al. (2018), BCC BCC-CSM2MR model output prepared for CMIP6 CMIP historical, <https://doi.org/10.22033/ESGF/CMIP6.2948>.
- Yu, Y. (2019), CAS FGOALS-f3-L model output prepared for CMIP6 CMIP historical, <https://doi.org/10.22033/ESGF/CMIP6.3355>.
- Yukimoto, S., T. Koshiro, H. Kawai, et al. (2019), MRI MRI-ESM2.0 model output prepared for CMIP6 CMIP historical, <https://doi.org/10.22033/ESGF/CMIP6.6842>.
- Zhang, J., R. Lindsay, M. Steele, and A. Schweiger (2008), What drove the dramatic retreat of arctic sea ice during summer 2007?, *Geophysical Research Letters*, 35(11), <https://doi.org/10.1029/2008GL034005>.
- Ziehn, T., M. Chamberlain, A. Lenton, et al. (2019), CSIRO ACCESS-ESM1.5 model output prepared for CMIP6 CMIP historical, <https://doi.org/10.22033/ESGF/CMIP6.4272>.
- Årthun, M., T. Eldevik, L. H. Smedsrud, Ø. Skagseth, and R. B. Ingvaldsen (2012), Quantifying the Influence of Atlantic Heat on Barents Sea Ice Variability and Retreat, *Journal of Climate*, 25(13), 4736–4743, <https://doi.org/10.1175/JCLI-D-11-00466.1>.